

# Disabling the Fanconi Anemia Pathway in Stem Cells Leads to Radioresistance and Genomic Instability

Xinzhu Deng<sup>1</sup>, Jason Tchieu<sup>2</sup>, Daniel S. Higginson<sup>3</sup>, Kuo-Shun Hsu<sup>1</sup>, Regina Feldman<sup>1</sup>, Lorenz Studer<sup>2</sup>, Shai Shaham<sup>4</sup>, Simon N. Powell<sup>3</sup>, Zvi Fuks<sup>3</sup>, and Richard Kolesnick<sup>1</sup>



## ABSTRACT

Fanconi anemia is an inherited genome instability syndrome characterized by interstrand cross-link hypersensitivity, congenital defects, bone marrow failure, and cancer predisposition. Although DNA repair mediated by Fanconi anemia genes has been extensively studied, how inactivation of these genes leads to specific cellular phenotypic consequences associated with Fanconi anemia is not well understood. Here we report that Fanconi anemia stem cells in the *C. elegans* germline and in murine embryos display marked nonhomologous end joining (NHEJ)-dependent radiation resistance, leading to survival of progeny cells carrying genetic lesions. In contrast, DNA cross-linking does not induce generational genomic

instability in Fanconi anemia stem cells, as widely accepted, but rather drives NHEJ-dependent apoptosis in both species. These findings suggest that Fanconi anemia is a stem cell disease reflecting inappropriate NHEJ, which is mutagenic and carcinogenic as a result of DNA misrepair, while marrow failure represents hematopoietic stem cell apoptosis.

**Significance:** This study finds that Fanconi anemia stem cells preferentially activate error-prone NHEJ-dependent DNA repair to survive irradiation, thereby conferring generational genomic instability that is instrumental in carcinogenesis.

## Introduction

The Fanconi anemia (FA; ref. 1) pathway, comprising 22 proteins in humans, regulates fundamental aspects of cellular function by coordinating DNA repair mechanisms as diverse as nonhomologous end joining (NHEJ), homology-directed repair (HDR), nucleotide excision repair, and interstrand cross-link (ICL) repair (1–3). Biallelic mutations in Fanconi anemia genes lead to Fanconi anemia, an inherited genomic instability syndrome considered a consequence of defective ICL repair. Homozygous individuals display congenital abnormalities, bone marrow aplasia, and cancer predisposition (4, 5). In mammals, DNA cross-link recognition by the FANCM protein recruits the Fanconi anemia core complex, and monoubiquitylation of FANCD2/FANCI then promotes DNA damage signaling and recruitment of downstream Fanconi anemia proteins and other repair enzymes (6). The genome of the nematode *C. elegans* contains at least five orthologs of mammalian Fanconi anemia genes [FANCD1 (BRCA2)/D2/I/J/M] (7), and as in mammals, FCD-2/FANCD2 is essential for crosslink-induced DNA damage repair in this animal. Loss-of-function (*lf*) mutations in *C. elegans fcd-2* result in hypersensitivity to cross-linking agents such as cis-diamminedichloroplatinum (CDDP) and mitomycin C (MMC; refs. 8, 9). Animals treated with these reagents exhibit high rates of progeny lethality at embryonic stages (8, 9), thought to reflect a high mutational load resulting from

inappropriate engagement of error-prone NHEJ in the mitotic stem cell compartment of the parental germline (9, 10). As in mammalian somatic cells, loss of Fanconi anemia signaling in *C. elegans* is thought to have little impact on radiation-induced DNA double-strand break (DSB) repair (8). How loss of Fanconi anemia genes results in specific phenotypic consequences in *C. elegans* and in mammals is not well understood. We therefore sought to track the etiology of organismal defects induced by Fanconi anemia mutations using the *C. elegans* germline (Supplementary Fig. S1) and murine embryonic stem (ES) cell models following exposure to different DNA-damaging agents.

## Materials and Methods

### Nematode strains

Wild-type N2, *ced-3(n717)*, *ced-4(n1162)*, *lig-4(ok716)*, *fcd-2(tm1298)*, *dog-1(VCI3)*, and *unc-58(e665)* strains were provided by the Caenorhabditis Genetics Center (The University of Minnesota, Minneapolis, MN). *unc-58(e665)* hermaphrodites were backcrossed 3× onto N2 before use. *glp-1(ar202)* was kindly provided by Iva Greenwald (Biological Sciences at Columbia University, New York, NY). Transgenic strain *smls76* was from Xue Ding (The University of Colorado, Boulder, CO) and strain *RW10105* was from Zhirong Bao (Memorial Sloan Kettering Cancer Center, New York, NY). Strains were maintained as per Brenner at 15°C (11). Experiments were performed at 20°C unless otherwise indicated. Double mutant *ced-3(n717);fcd-2(tm1298)*, *ced-4(n1162);fcd-2(tm1298)*, *glp-1(ar202);fcd-2(tm1298)*, *lig-4(ok716);fcd-2(tm1298)*, *fcd-2(tm1298);smls76*, *ced-3(n717);fcd-2(tm1298);smls76*, *fcd2(tm1298);RW10105*, *ced-3(n717);fcd2(tm1298);RW10105*, and *fcd-2(tm1298);unc-58(e665)* worms were generated by standard genomic methodology using PCR, genomic DNA sequencing in *ced-4(n1162)*, or by examining specific established mutant phenotypes in *glp-1(ar202)* [it forms a germline stem cell (GSC) tumor at 25°C] (12) and *unc-58(e665)* (paralysis; ref. 13), or reporter gene expression in the transgenic strains *smls76* (14) and *RW10105* (15). For example, a double mutant *lig-4(ok716);fcd-2(tm1298)* was isolated and genotyped using two sets of PCR primers designed according to the DNA sequence of the deletion allele *lig-4(ok716)* and *fcd-2(tm1298)* (Supplementary Fig. S2A and S2B). PCR

<sup>1</sup>Laboratory of Signal Transduction, Memorial Sloan Kettering Cancer Center, New York, New York. <sup>2</sup>Center for Stem Cell Biology, Memorial Sloan Kettering Cancer Center, New York, New York. <sup>3</sup>Department of Radiation Oncology, Memorial Sloan Kettering Cancer Center, New York, New York. <sup>4</sup>The Rockefeller University, New York, New York.

**Note:** Supplementary data for this article are available at Cancer Research Online (<http://cancerres.aacrjournals.org/>).

**Corresponding Author:** Richard Kolesnick, Laboratory of Signal Transduction, Memorial Sloan-Kettering Cancer Center, 1275 York Ave, New York, NY 10065. Phone: 646-888-2174; E-mail: r-kolesnick@ski.mskcc.org

Cancer Res 2021;81:3706–16

doi: 10.1158/0008-5472.CAN-20-3309

©2021 American Association for Cancer Research

primers for distinguishing mutant *fcd-2(tm1298)* from wild-type are 5' gagaagagaattggaggcagaa 3'/5' tgacagattgaagttcatcgca 3'; for genotyping mutant *lig-4(ok716)* are 5' tgcaaacaaaattcgatggag 3'/5' cttttgtcttttggccact 3' and for wild-type *lig-4* are 5' cagattgaaaagttggaggctc 3'/5' tcaagaattgttgaatgtcctc 3'; PCR primers for genotyping mutant *ced-3(n717)* are 5'-cggcttcttctccacacttgta-3'/5'-ggcgcacacc-catttgattg-3' and for wild-type *ced-3* are 5'-cggcttcttctccacacttgta-3'/5'-ggcgcacaccatttgattg-3'; for genotyping mutant *glp-1(ar202)* are 5' ttggagaatggcttttct 3'/5' gtcatacaatacaatccgtg 3' and for wild-type *glp-1* are 5' ttggagaatggcttttccc 3'/5' gtcatacaatacaatccgtg 3'.

### C. elegans RNAi

Single colonies of HT115 bacteria containing L4440 plasmids with cloned fragments corresponding to target genes were from Vidal and Ahringer RNAi feeding libraries. RNAi by feeding was performed essentially as described previously (16).

### ICL agent treatment in C. elegans

CDDP (Sigma) and MMC (Sigma) were dissolved in water and diluted in M9 buffer (22 mmol/L KH<sub>2</sub>PO<sub>4</sub>, 42 mmol/L NaHPO<sub>4</sub>, 85.6 mmol/L NaCl, 1 mmol/L MgSO<sub>4</sub>) to the desired concentrations. Worms were synchronized and soaked in CDDP or MMC at the indicated doses and times at 20°C. After treatment, worms were transferred to Nematode Growth Medium (NGM) plate to recover prior to phenotype analysis.

### C. elegans germ cell quantification

Worms were fixed in ethanol and stained with 4',6-diamidino-2-phenylindole (DAPI) using Vectashield (Vector Laboratories, Inc.). Z-stack images of DAPI-stained gonads were acquired with a 20× objective at 2 μm intervals using a Leica Confocal Microscope. Number of germ nuclei in one gonad arm was quantified using Volocity Software (version 6.3), as described previously (17). To study mitotic germ cell sensitivity to DNA damage, L4 larvae of *glp-1(ar202)(GC833)* raised at 15°C were shifted to 25°C and progeny were collected for experiments.

### C. elegans germ cell and embryo cell death quantification

DNA damage-induced germ cell apoptosis was studied, as described previously (17). After L4 stage, worms were treated with Cs<sup>137</sup> radiation or ICL agents, germ cell corpses were scored in the distal pachytene region of one gonad arm using DIC optics. Transgenic strain *smls76 (PhspAnxV::GFP)* was used to visualize apoptotic cells in *C. elegans* embryos as published previously (14). Adult hermaphrodites were incubated at 33°C for 45 minutes to induce expression of sAnxV::GFP fusion proteins. After heat shock, worms were transferred to OP50 bacteria seeded plates for embryo collection. Apoptotic cells were examined for the presence of the sAnxV::GFP in staged embryos using a Zeiss Axioplan 2 microscope equipped with epifluorescence filters, as described by Mapes and colleagues. (14). Transgenic strain RW10105 (zul178 [his-72(promoter)::his-72::GFP+unc-119(+); stf1s?? [pha-4(promoter)::his-72::dsRed+unc-119(+)] was used to measure embryonic cell loss after CDDP treatment.

### DNA damage-induced oocyte chromosome aberrations

To measure *C. elegans* mitotic germ cell ICL sensitivity, 20–30 young adult hermaphrodites were seeded into each well of a 12-well culture plate containing 0.5 mL CDDP solution. After soaking for 4 hours, worms were transferred to NGM plate to recover at 20°C for 16 hours, and followed by DAPI staining; for UVA sensitivity, L4 stage worms were treated with 2 μg/mL trioxalen (4,50,8-trimethylpsoralen,

Sigma-Aldrich) in an Eppendorf tube prepared by diluting 3 mg/mL trioxalen in DMSO with M9 solution. The tube was wrapped in aluminum foil and incubated on a rocker at low speed for 1 hour. Following trioxalen treatment, worms were transferred to a fresh OP50 bacteria-seeded plate, irradiated using a XL-1000 Spectrolinker UVA light (800J, 365 nm UVA lamp, Spectroline com.) at 1 μW/cm<sup>2</sup>, and collected at 24 hours for DAPI staining. Z-stack images were acquired with a 63× objective at 0.25 μm intervals using a Leica Confocal Microscope. For each worm, two oocytes (−1 and −2 position distal to the spermatheca) in one side of the gonad were scored for chromosome aberrations through three-dimensional data stacks of whole nuclei. ICL-induced nuclear aberrations include an abnormal number of DAPI-stained bodies (> or < 6, representing dissociated bivalents or clumped chromosomes) and chromosome fragmentation and filament structure.

### C. elegans embryo survival

Young adult hermaphrodites were exposed to the indicated doses of radiation, or ICL agents for 16 hours by soaking, as described above. Treated worms were transfer to NGM plates (1 worm/plate) to collect eggs. Number of eggs laid was scored 24 hours after treatment, and unhatched eggs were scored the next day. Embryonic survival was calculated as number of total eggs divided by number of hatched eggs.

### Functional assay for genomic instability

Functional genomic instability was measured using *C. elegans* strain CB665 [genotype *unc-58(e665)X*] as described by Harris (18) and Huuononen (19). The principle of this assay is that the “paralysis” phenotype of *unc-58(e665)* can be reversed to a wild-type phenotype caused by spontaneous *unc-58(e665)* intragenic and extragenic suppressor mutations. Briefly, synchronized L4 larvae were soaked in CDDP at the indicated doses for 14 hours at 20°C or irradiated with 2 Gy. After treatment, five P<sub>0</sub> worms were transferred to a 60-mm plate allowing worms to lay eggs for 3 days and P<sub>0</sub> animals were removed afterward. A total of 40 plates was used per group. Four F1 progeny were dispensed to a fresh 60-mm plate on day 4 as they aged to L3–L4. Each of the 40 original plates produced five plates and a total of 200 plates were made for each group. After 4 weeks at 20°C, starved worms are transferred in agar chunks to the center of 100-mm plates seeded with OP50 bacteria in a 0.5-cm-thick ring at the edge of the plate. Mobile revertants crawl quickly over to the bacteria ring and are easily scored in first culture as revertants on day 2 after transfer. A second culture was generated by randomly recovering worms from 40 of 100-mm plates from the first culture without revertants. Five L3–L4 larvae were then dispensed to one of fresh 60-mm plates and total 200 plates were generated for each group. Plates were cultured at 20°C and revertant rate was scored after 4 weeks, as described above.

### Murine ES cell culture

*FancD2*-mutant murine ES cell FANCD2 #3 and FANCD2 #4, and wild-type J1 cells, were provided by Markus Grompe (Oregon Health & Science University, Portland, OR). Cells were grown on gelatinized plates without feeder in Knockout DMEM (Gibco/Thermo Fisher Scientific) supplemented with 15% ES cell-qualified FBS (Gemini), 2 mmol/L L-glutamine, 1× MEM Non-Essential Amino Acids, 55 μmol/L β-mercaptoethanol, and 1,000 U/mL LIF (Chemicon/Millipore, Sigma) in a 37°C humidified atmosphere under 5% CO<sub>2</sub>.

### Murine ES cell γH2AX focus analysis

Mouse ES cells, plated on coverslips, were subjected to 5 Gy and thereafter incubated for the indicated times before fixation with 4%

Deng et al.

paraformaldehyde. Fixed cells were quenched with 50 mmol/L NH<sub>4</sub>Cl for 5 minutes, washed three times with PBS, blocked in Blocking Buffer (PBS with 0.5% BSA, 0.02% Na-azide, 0.36 μmol/L DAPI and 0.25% Triton X-100) for 30 minutes, and then incubated with mouse anti-phospho-H2AX-Ser139 primary Ab (Millipore, clone JBW301, 1:500 dil) in fresh Blocking Buffer for 1 hour. After three PBS washes (5 minutes each), cells were incubated with the Alexa Fluor 488-Alexa-dye-conjugated secondary antibody (Thermo Fisher Scientific, catalog no. A21202, 1:400) in fresh Blocking Buffer for 40 minutes. After three PBS washes, coverslips were mounted with ProLong Dimond Antifade solution. Fluorescent images of five serial sections spanning 1 μm thickness were acquired with a 63×/1.4NA objective oil lens, images were deconvoluted using AutoQuant X, and max-projected into a single image using Image J. Nuclear foci were determined by a threshold set in Image J and scored manually using 8.28 pixels as average focus size based on discreet γH2AX foci generated at a low radiation dose (2 Gy at 30 minutes) as published previously (20). A cell containing > 5 foci was considered positive. For each data point, at least 163 (and up to 340) cells were analyzed.

### Murine ES cell clonogenic survival assay

Cells were trypsinized and resuspended in complete media at 1 × 10<sup>6</sup> cells/mL in a 15 mL tube. Cells were irradiated and then plated onto gelatinized dishes in triplicate at varying cell concentrations using complete media. Media were changed every day and surviving colonies (>50 cells) were fixed with 1% glutaraldehyde and stained with Trypan Blue at day 4 or day 5 after radiation. For MMC treatment, trypsinized cells were resuspended in complete media and plated onto gelatinized dishes in varying cell numbers. After adhering overnight, ES cell media was replaced with MMC-containing media. After 48 hours treatment, cells were fed with fresh ES cell media and handled as above. Surviving fraction was calculated as number of colonies formed per number of cells seeded × plating efficiency (21). Radiation dose survival curves were fitted to the standardized single-hit multi-target model using GraphPad Prism 6. D0 and Dq were calculated as described previously (22).

### DNA damage-induced ES cell apoptosis

Apoptosis was assessed *in vitro* by examining morphologic changes in nuclear chromatin (23). After exposure to DNA-damaging agents, ES cells were collected at the indicated times, followed by fixing with 2% paraformaldehyde, two washes in PBS, and staining with 100 μL of 24 μg/mL bis-benzimidazole trihydrochloride solution (Hoechst #33258; Sigma-Aldrich) for 10 minutes.

### XRCC4 short hairpin RNA in mouse ES cells

Murine XRCC4 short hairpin RNAs (shRNA) were identified using the Department of Scientific and Industrial Research website. Highest scoring hairpins were cloned into the doxycycline-inducible lentiviral shRNA construct pTRIPZ. After sequence verification of shRNA constructs, lentivirus was produced using 293T cells and concentrated. Virus was added to ES cells overnight with 4 μg/mL polybrene to enhance delivery. Thereafter, viral supernatant was replaced with normal ES cell media and after 24 hours, cells were subjected to puromycin (2 μg/μL) selection. Colonies were selected and maintained in puromycin for the duration of the selection process. To determine level of knockdown, puromycin was removed, and 1 μg/μL doxycycline or H<sub>2</sub>O control were added to cells. RFP expression appeared within 24 hours. Cells were incubated in doxycycline for 72 hours and harvested for RNA/protein expression analysis. Mouse XRCC4 expression level was standardized to mouse hypoxanthine guanine

phosphoribosyl transferase expression (Open Biosystems). Standard Western blots were performed and probed for XRCC4, and mouse HSP90 as loading controls.

### Statistical analysis

Statistical significance was determined by two-tailed Student *t* test or  $\chi^2$  test using GraphPad Prism software (GraphPad). Results are presented as mean ± SEM. The *P* value in the mouse clonogenic ES cell survival assay was calculated as per 95% confidence intervals defined by Altman and Bland (24).

## Results

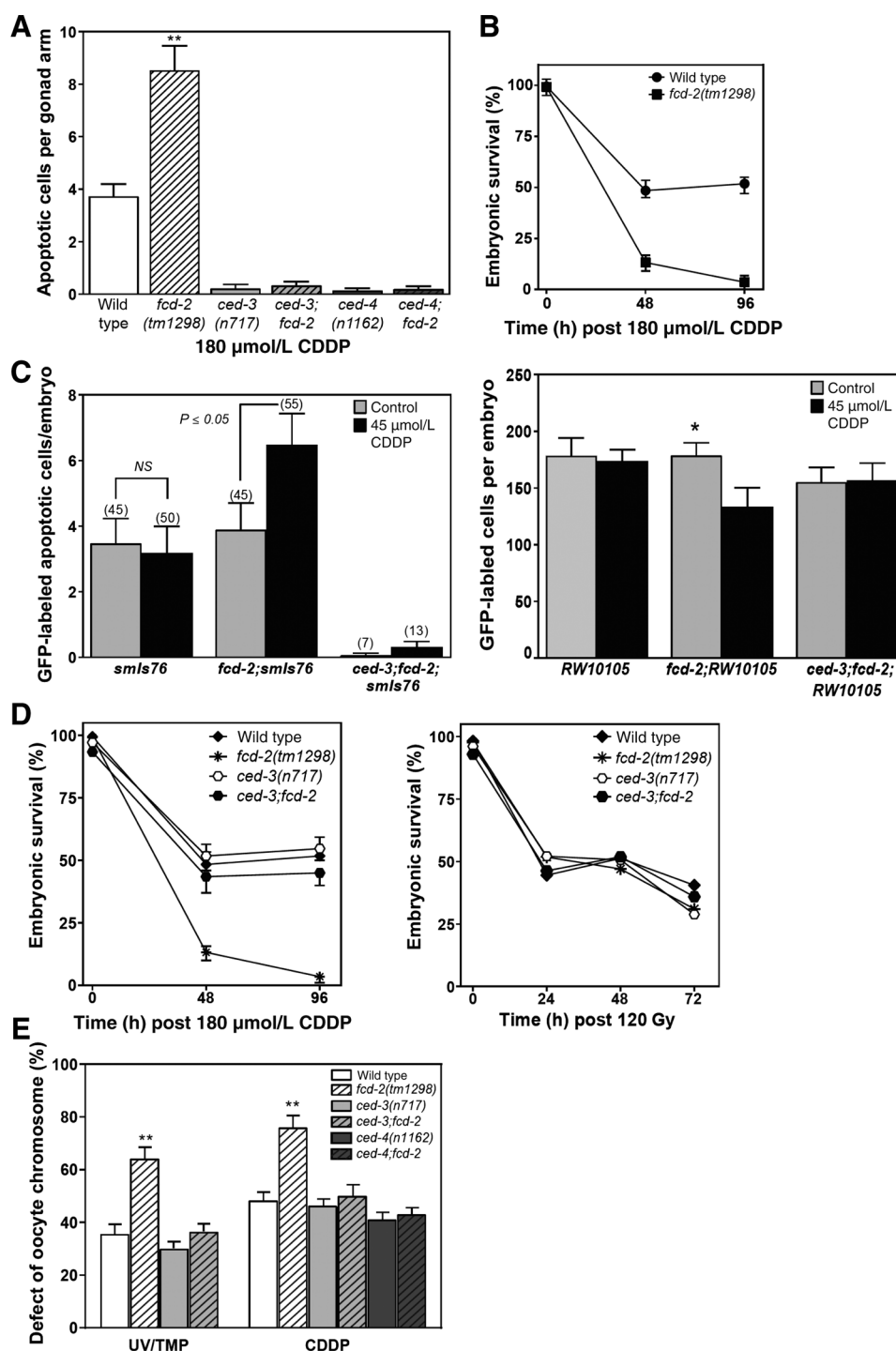
Previous studies (9, 25), confirmed here (Fig. 1A; Supplementary Fig. S3), demonstrate that cross-linking agents enhance NHEJ-dependent apoptosis in the pachytene meiotic zone of developing *C. elegans*. We wondered, therefore, whether embryonic lethality in progeny of treated animals, might also reflect inappropriate cell death activation. To test this idea, we first confirmed that the *fcd-2(tm1298)* mutation or *fcd-2* knockdown by RNAi indeed exacerbate progeny lethality following parent treatment with CDDP (Fig. 1B; Supplementary Fig. S4) or MMC (Supplementary Fig. S5). Next, we examined animals expressing a sAnxV::GFP(*smIs76*) transgene, encoding a secreted protein fragment recognizing exposed phosphatidylserine on dying cell corpses, an established model to quantify apoptotic cells in the *C. elegans* gonad (14). We found that baseline number of GFP-labeled dying cells in wild-type progeny embryos was unaffected following CDDP treatment of their parents. However, progeny of CDDP-treated *fcd-2(tm1298);smIs76* animals exhibit nearly double the number of cell corpses (Fig. 1C, left). To confirm excess embryonic cell loss in *fcd-2(tm1298)* progeny of CDDP-treated animals, we examined embryos expressing a ubiquitous histone::GFP nuclear reporter (*RW10105*), which produces a histone::GFP nuclear reporter protein in every cell (15). We found significantly fewer cells in treated *fcd-2(tm1298);RW10105* mutants than in treated wild-type animals (Fig. 1C, right; *P* < 0.05).

To determine whether ICL hypersensitivity in Fanconi-deficient embryos is due to induction of an apoptotic program, we examined *fcd-2(tm1298)* animals also carrying the *ced-3(n717)* mutation, which inactivates the main *C. elegans* apoptotic caspase gene. We found no baseline cell corpse accumulation in these double mutants using the sAnxV::GFP reporter. Strikingly, loss of either *ced-3* or *ced-4*, encoding an Apaf-1-related caspase activator, prevents CDDP-induced apoptosis (Fig. 1C; Supplementary Fig. S6) and rescues enhancement of embryonic lethality accompanying *fcd-2* loss (Fig. 1D, left; Supplementary Fig. S7). Similarly, worms carrying a *lf* allele for DOG-1/FANCI, *dog-1(gk10)*, reported to confer ICL hypersensitivity (26) display increased CDDP-induced germ cell apoptosis and embryonic lethality, both abrogated by *ced-3* or *ced-4* RNAi (Supplementary Fig. S8A and S8B). In contrast, *ced-3* inactivation has no impact on radiation-induced embryonic sensitivity (Fig. 1D, right). Although ionizing radiation-induced apoptotic death in *C. elegans* germ cells requires CEP-1/p53-mediated upregulation of the BH3-only proteins, EGL-1 and CED-13, to activate the core apoptotic machinery (CED-9, CED-4, and CED-3; ref. 27), CDDP-induced hypersensitivity to germ cell apoptosis and embryonic lethality appear *cep-1/p53* independent in the *fcd-2* mutant (Supplementary Fig. S9A and S9B). Ongoing investigations in our lab are currently screening for genes involved in Fanconi anemia ICL hypersensitivity to apoptosis in the *C. elegans* germline.

To uncover the maternal defects leading to embryonic lethality, we examined diakinesis oocytes of animals of various genotypes following

**Figure 1.**

Apoptosis mediates FANCD2 deficiency-induced ICL sensitivity. **A**, Enhanced CDDP (180  $\mu\text{mol/L}$ )-induced germ cell apoptosis (at 48 hours) in *C. elegans fcd-2*-deficient worms is blocked by inactivating *ced-3/ced-4*. \*\*,  $P \leq 0.01$ . **B**, FCD2 deficiency increases CDDP-induced embryonic lethality. Late L4-stage wild-type and *fcd-2*-mutant *C. elegans* hermaphrodites were treated with 180  $\mu\text{mol/L}$  CDDP for 16 hours. Progeny survival was scored at 48 and 96 hours post-treatment ( $P \leq 0.01$  wild-type vs. *fcd-2* mutant). **C**, If *fcd-2* sensitizes CDDP-induced embryonic apoptosis. Left, embryos (number in parentheses) from late L4-stage worms treated with 45  $\mu\text{mol/L}$  CDDP for 6 hours, followed by 20 hours recovery, were collected at 2 hours after egg laying to detect sAnxV::GFP-expressing apoptotic cells. Right, If *fcd-2* sensitizes CDDP-induced embryonic cell loss, quantified in GFP-reporter strains *RW10105*, *fcd-2;RW10105*, and *ced-3;fcd-2;RW10105*. \*,  $P \leq 0.05$ . **D**, If *ced-3* blocks 180  $\mu\text{mol/L}$  CDDP (at 16 hours)-enhanced (left), but not 120 Gy (right)-induced, lethality in embryos isolated from late L4 stage-treated *fcd-2* mutants. **E**, UV- and CDDP-induced chromosomal abnormality increases in *fcd-2*-mutant oocytes are blocked by inhibiting apoptosis. L4-stage worms were exposed to photoactivated 4,5,8-trimethyl psoralen [TMP (2  $\mu\text{g/mL}$ )+UVA (800J)], or 180  $\mu\text{mol/L}$  CDDP, for 16 hours. Diakinesis-oocyte chromosome abnormalities were detected as in Materials and Methods. \*\*,  $P \leq 0.01$ .



cross-link induction with either photoactivated psoralen or CDDP. As before, animals were treated in the L4 stage, before meiosis and oocyte production has occurred. Wild-type oocytes visualized with DAPI usually present six bivalent chromosomes, corresponding to six paired homologs attached by chiasmata. DNA damage can lead to bivalent dissociation, clumping, or fragmentation (25). We found, as published previously (9), that *fcd-2* mutant oocytes exhibit more chromosome damage than wild-type animals following treatment (Fig. 1E;  $P < 0.002$

for trimethylpsoralen;  $P < 0.01$  for CDDP), an event mediated by NHEJ (9). This increased chromosomal damage, like embryonic lethality, is entirely reversed in *ced-3;fcd-2* or *ced-4;fcd-2* double mutants. While it seems unlikely that oocytes displaying massive chromosomal damage would be viable, we posit that increased embryonic lethality in *fcd-2* mutants likely reflects more modest ectopic caspase activation in the maternal germline, yielding transmissible chromosome damage that leads to embryonic cell death and embryo

lethality. Alternately, *fcd-2*-mutant oocytes with modest numbers of cross-links might be sufficiently viable to be fertilized, but once the stress of embryo cell division occurs these unresolved crosslinks would initiate NHEJ-dependent apoptosis. In either case, ultimately embryonic lethality reflects enhanced apoptosis.

The embryo and oocyte defects we studied are likely consequences of damage inflicted on GSCs, as GSCs in L4-treated animals in our studies have yet to undergo meiosis and oocyte formation. We sought, therefore to determine whether Fanconi anemia genes have direct effects on *C. elegans* GSCs. We found that the cross-linking reagents CDDP and MMC reduce mitotic GSC compartment size of wild-type and *fcd-2(tm1298)* mutants to similar extents (Fig. 2A, left and right, respectively), as assessed by counting mitotic GSC nuclei. Supporting this observation, the *fcd-2(tm1298)* mutation does not alter GSC sensitivity in animals also carrying the *glp-1(ar202)* mutation, which causes an expanded mitotic germ cell compartment (12), allowing for more quantitative scoring of perturbations (Fig. 2B). These observations suggest that inappropriate NHEJ upon *fcd-2* loss leads to DNA repair with residual structural damage that does not engage the apoptotic machinery in *C. elegans* GSCs, but only in oocytes they generate. These results are supported by our previous findings that apoptosis is inactive in GSCs (17).

To determine whether *fcd-2* may be required for repair of other DNA lesions in GSCs, we examined GSC responses to ionizing radiation. Surprisingly, we found that while *fcd-2(tm1298)* does not exacerbate progeny lethality following parental irradiation (Fig. 1D; refs. 8, 25), loss of *fcd-2* renders mitotic GSCs in *glp-1(ar202)* mutants radiation resistant (Fig. 2C, left) over a range of 60–180 Gy. For example, at 48 hours following 120 Gy, *glp-1(ar202);fcd-2(tm1298)* animals possess  $1,950 \pm 187$  nuclei per gonad arm compared with  $1,216 \pm 125$  in *glp-1(ar202)* single mutants ( $P < 0.001$ ). Similar findings were observed in wild-type versus *fcd-2(tm1298)*-mutant comparisons (Fig. 2C, right). This resistance appears to be mediated by NHEJ activation, as the approximately 40% radioresistance imparted by *fcd-2(tm1298)* to otherwise wild-type animals is abrogated by a *lf* mutation in the NHEJ gene *lig-4* (Fig. 2C, right). Because *lig-4* mutations alone do not affect wild-type GSC radiation sensitivity (Fig. 2C, right), our results suggest that loss of *fcd-2* inappropriately triggers NHEJ activation, leading to ionizing radiation resistance. Thus, in the presence of ionizing radiation, *fcd-2* is required normally to keep NHEJ in the “off” state in GSCs.

Although *fcd-2* does not play a role in embryonic lethality induced following ionizing radiation, we reasoned that GSCs surviving irradiation in *fcd-2* mutants, may give rise to progeny carrying a higher mutational load. An extensive literature indicates that NHEJ-dependent DSB repair pathways (cNHEJ and alt-NHEJ), such as those inappropriately activated in animals with Fanconi anemia, are error prone, with initiating lesions establishing a mutator state of genomic instability propagated through progeny (28, 29). A previous study reported that progeny of X-ray irradiated *unc-58(e665)* animals show a low-level increase in mutation frequency over background, as assessed by reversion of the uncoordinated locomotion and body-shape defects of these animals, with a maximal mutation rate induced between 1 and 3 Gy (19). We therefore irradiated *unc-58(e665)* animals at 2 Gy, and scored revertant frequency in three independent trials. While we did not observe significant increase in mutation frequency in descendants of irradiated wild-type animals (0.89 vs. 0.17,  $P = 0.112$ ), progeny of *fcd-2* mutants displayed markedly increased revertant frequencies, with a pooled rate of 3.98%, >10-fold higher than the unirradiated *fcd-2* mutant rate of 0.34% ( $P \leq 0.0001$ ) and almost 5-fold of

irradiated wild-type controls ( $P < 0.004$ ; Fig. 3). Of note, CDDP treatment does not significantly increase *unc-58(e665)* reversion frequency in an *fcd-2*-deficient background (Fig. 3), consistent with the possibility that genomically altered embryos die by apoptosis activation, are not identifiable in the current assay, and hence are not represented in the descendent population.

Our findings so far suggest a model (Supplementary Fig. S10) in which loss of *fcd-2* differentially affects GSC responses to DNA-damaging agents. In *fcd-2* mutants, inappropriate NHEJ repairs ICL intermediates but leaves residual structural damage that yields chromosomal aberrations in progeny oocytes, leading to embryonic cell apoptosis and embryo lethality. In response to ionizing radiation, however, *fcd-2* deficiency leads to NHEJ repair with errors in GSCs without subsequent apoptosis. This results in persistence of oocytes and embryonic cells with high mutagenic load.

To explore generality of our findings, we sought to determine whether different DNA-damaging agents have differential effects on wild-type mouse J1 ES cells and two ES cell lines derived from *Fancd2*-null mice (kindly provided by Markus Grompe; ref. 30). Consistent with our *C. elegans* findings, upon treatment with escalating doses of MMC, *Fancd2*-mutant ES cells displayed significantly-reduced colony formation, with cell line #4 failing to form colonies even at the lowest dose of 40 nmol/L MMC (Fig. 4A). Colony formation appeared to correlate with cell death induction. At 320 nmol/L MMC, 34% of wild-type J1 cells died, whereas 70% and 97% of FANCD2 #3 and FANCD2 #4 ES cells, respectively, died (Fig. 4B). Importantly, cell death was apoptotic, as the pan-caspase inhibitor ZVAD blocked MMC-induced cell death in all ES cell lines (Fig. 4C). Furthermore, NHEJ downregulation by shRNA-mediated inactivation of XRCC4, a LIG4 cofactor, selectively blocked apoptosis enhancement after MMC treatment in FANCD2 *lf* cell lines (Fig. 4D). These studies support the existence of two separate mechanisms for apoptosis induction by MMC in ES cells: a baseline NHEJ-independent mechanism, and a FANCD2-repressed NHEJ-dependent pathway, revealed only by *Fancd2* loss.

Mouse ES cells predominantly utilize high-fidelity HDR and not NHEJ to repair DNA DSBs (31), suggesting possible similarities with *C. elegans* GSCs. Indeed, we found that, like *C. elegans* GSCs, both murine ES cell lines lacking FANCD2 exhibit ionizing radiation resistance (Fig. 4E, left), as assessed by a clonogenic survival assay widely employed for defining dose-survival of eukaryotic cells. While D0 values (the dose required for 37% survival) were similar for all three cell types ( $1.48 \pm 0.11$  Gy-wild type,  $1.56 \pm 0.22$  Gy-FANCD2 #3,  $1.75 \pm 0.41$  Gy-FANCD2 #4), the Dq value, which represents the dose threshold preceding the linear relationship between dose and cell survival, for J1 ES cells was zero, while FANCD2 #3 and FANCD2 #4 ES cell lines displayed Dq values of  $1.77 \pm 0.7$  Gy and  $1.38 \pm 1.0$  Gy, respectively ( $P < 0.01$  each vs. J1). Consistent with our observations of *C. elegans* GSCs, downregulation of XRCC4 (Supplementary Fig. S11A and S11B) restores radiosensitivity to the FANCD2-deficient ES cells (Fig. 4E, right), without increasing baseline wild-type radiosensitivity.

To formally show that NHEJ-dependent radioresistance as measured by clonogenic survival assay reflects enhanced DNA damage repair, we employed  $\gamma$ H2AX focus technology. Accrual and resolution of  $\gamma$ H2AX foci at the site of DSBs is widely regarded as a surrogate for number and resolution of DSBs, respectively (32). Whereas  $\gamma$ H2AX foci are almost undetectable prior to irradiating wild-type or Fanconi anemia ES cells, at 0.5 hours post 5 Gy, the point of maximal accrual of  $\gamma$ H2AX foci, 90%–95% of wild-type and Fanconi anemia ES cells display  $\gamma$ H2AX foci ( $56 \pm 4$  foci/WT ES cells;  $58 \pm 3$  foci/FANCD2 #3

## FA Stem Cells Radioresistance Yields Genomic Instability

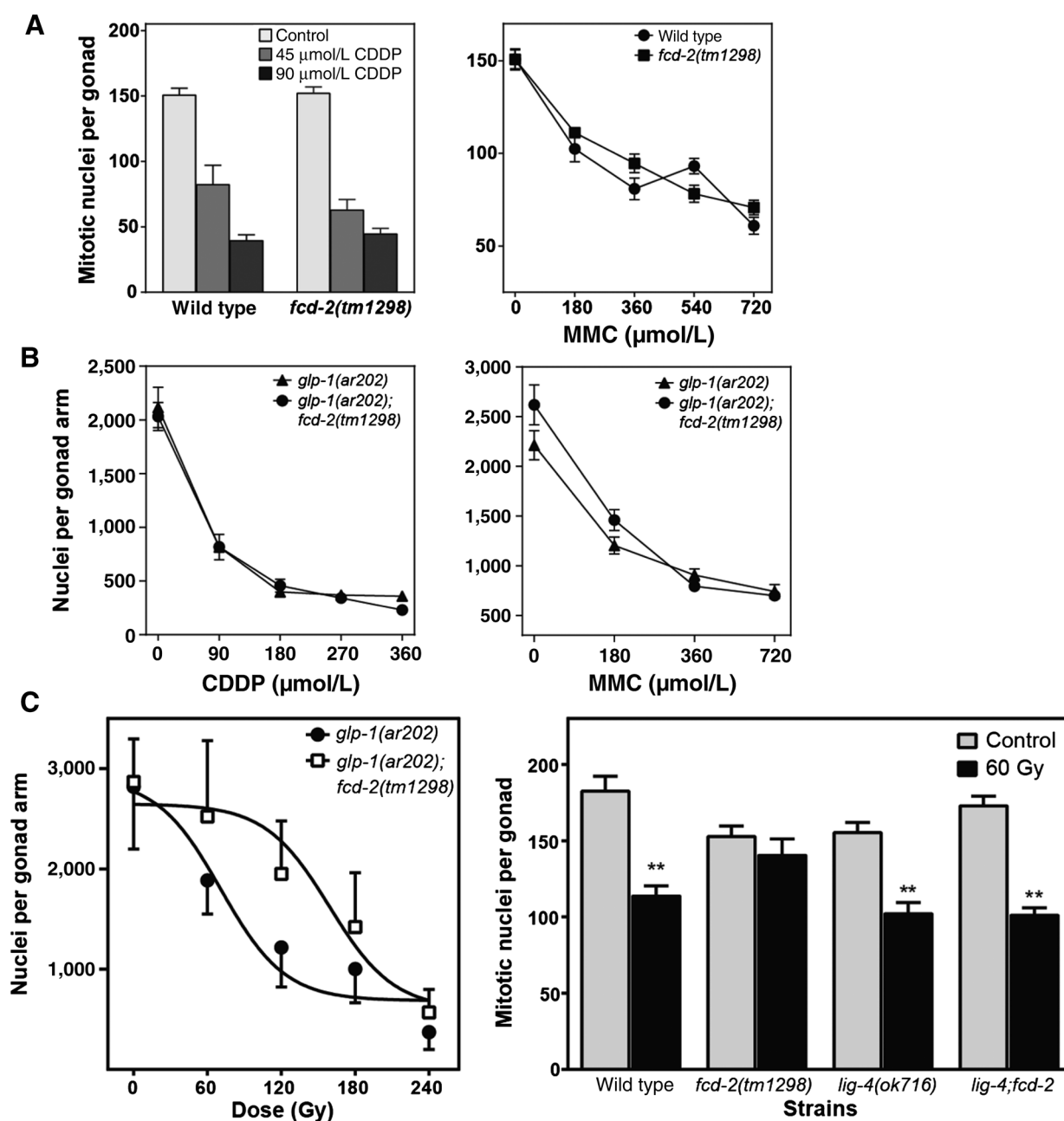


Figure 2.

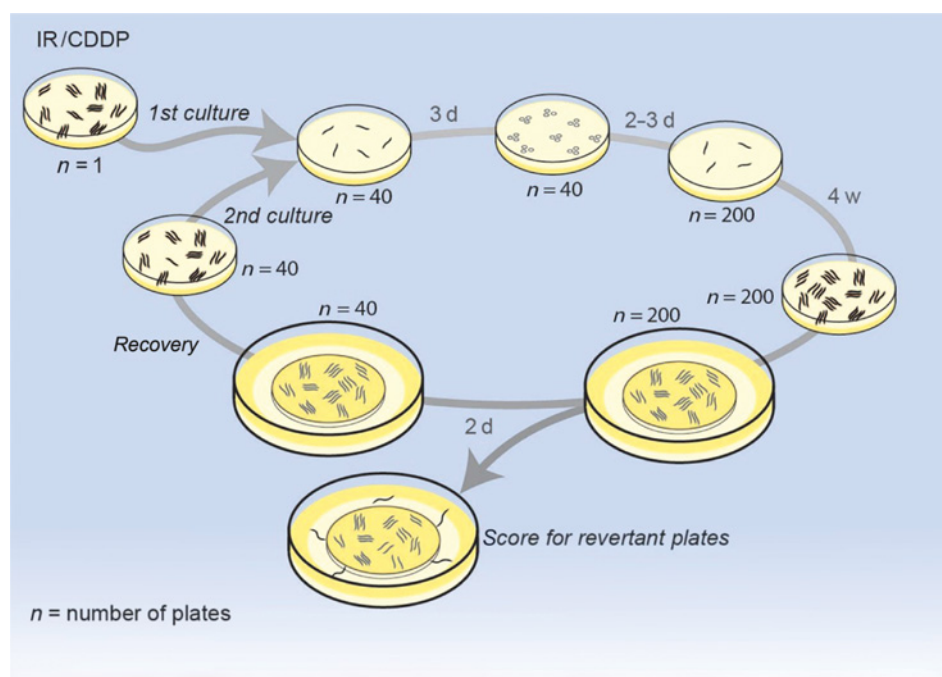
*C. elegans* FANCD2 deficiency does not impact ICL sensitivity of mitotic germ cells but yields NHEJ-dependent radiation resistance in stem cell populations. **A**, Late L4-stage wild-type and *fcd-2*-mutant worms were treated with indicated doses of CDDP (left) and MMC (right) for 16 hours and germline nuclei were quantified after 36 hours recovery from ICL treatment. **B**, L4 *glp-1(ar202)* and *glp-1(ar202); fcd-2(tm1298)* worms were treated with indicated doses of ICL agents CDDP (left) and MMC (right) for 16 hours and germline nuclei were quantified after 30 hours recovery from ICL treatment. **C**, Mitotic GSCs in *C. elegans* display NHEJ-dependent radiation resistance. Left, *glp-1(ar202)* and *glp-1(ar202); fcd-2(tm1298)* adults were shifted from the permissive (15°C) to restrictive temperature (25°C) and late-L4 progeny were irradiated. Mitotic GSCs in distal and proximal regions were quantified after 48 hours. Right, late L4 worms were left unirradiated (gray) or irradiated with 60 Gy (black), and gonadal mitotic nuclei in the distal gonad were quantified after 42 hours. \*\*,  $P < 0.01$  versus unirradiated. Data (mean  $\pm$  SEM) are from 6 to 9 worms per group (**A**), or from  $\geq 9$  worms per group (**B** and **C**).

ES cells and  $58 \pm 4$  foci/FANCD2 #4 ES cells; Fig. 5A and B). Thereafter, consistent with accelerated DNA repair, Fanconi anemia ES cells resolve  $\gamma$ H2AX foci at an enhanced rate compared with wild-type ES cells.

## Discussion

Our results suggest that ICLs in *Fancd2*-mutant cells can lead to utilization of NHEJ in all cells and apoptotic lethality in progeny cells. Likewise, *Fancd2*-mutant stem cells when exposed to radiation fail to

Deng et al.

**Figure 3.**

Ionizing radiation increases mutation frequency in progeny of *fcd-2(tm1298)*. Revertants were scored in *unc-58(e665)* and *fcd-2(tm1298);unc-58(e665)* worms followed for >10 generations of two culture periods after CDDP or 2 Gy exposure, as described in Materials and Methods. Data were compiled from two experiments for CDDP and three experiments for ionizing radiation. One-tailed *P* value was derived using GraphPad Fisher exact test.

<i>unc-58 (e665)</i> background	CDDP ( $\mu\text{mol/L}$ )	IR (Gy)	Plates with revertants /total plates	Frequency of mutation (%)	<i>P</i> WT vs. <i>fcd-2</i> 0 Gy vs. 2 Gy	
Wild type	0		1/205	0.49	0.460	
<i>fcd-2(tm1298)</i>	0		2/188	1.06		
Wild type	3		1/212	0.47	0.480	
<i>fcd-2(tm1298)</i>	3		2/202	0.99		
Wild type	15		3/189	1.58	0.470	
<i>fcd-2(tm1298)</i>	15		2/200	1.00		
Wild type	45		1/215	0.47	0.470	
<i>fcd-2(tm1298)</i>	45		2/201	0.99		
Wild type		0	1/594	0.17	0.490	0.112
<i>fcd-2(tm1298)</i>		0	2/587	0.34		0.0001
Wild type		2	5/559	0.89	0.004	
<i>fcd-2(tm1298)</i>		2	22/553	3.98		

undergo apoptosis, but survive, likely accumulating genomic perturbations, dependent on NHEJ. Our findings may have important implications for the etiology of different physiologic failures associated with Fanconi anemia. We posit that predisposition to cancer in human patients with Fanconi anemia, exemplified by the long-term hazard of developing leukemia and solid tumors (33), in particular squamous carcinoma of the head and neck and anal cancer (34), may reflect inappropriate error-prone repair of DNA breaks by NHEJ in specific tissue stem cells. Congenital abnormalities and bone marrow failure observed in human patients with Fanconi anemia; however, may be an outcome of excessive apoptosis, perhaps through endogenous gener-

ation of aldehyde byproducts of cellular metabolism (35). In this context, it is of note that knockdown of the zebrafish homolog of human FANCD2 causes massive p53-mediated apoptosis during cellular proliferation (36). Our studies suggest that treatment approaches to Fanconi anemia pathologies may eventually need to be tailored to separately address the distinct mechanisms that produce the different components of the disease (37).

The current studies represent the discovery of a previously unrecognized mechanism for induction of radiation resistance involving inappropriate utilization of NHEJ, likely confined to stem cells. In this context, a substantial body of evidence indicates that neither murine

## FA Stem Cells Radioresistance Yields Genomic Instability

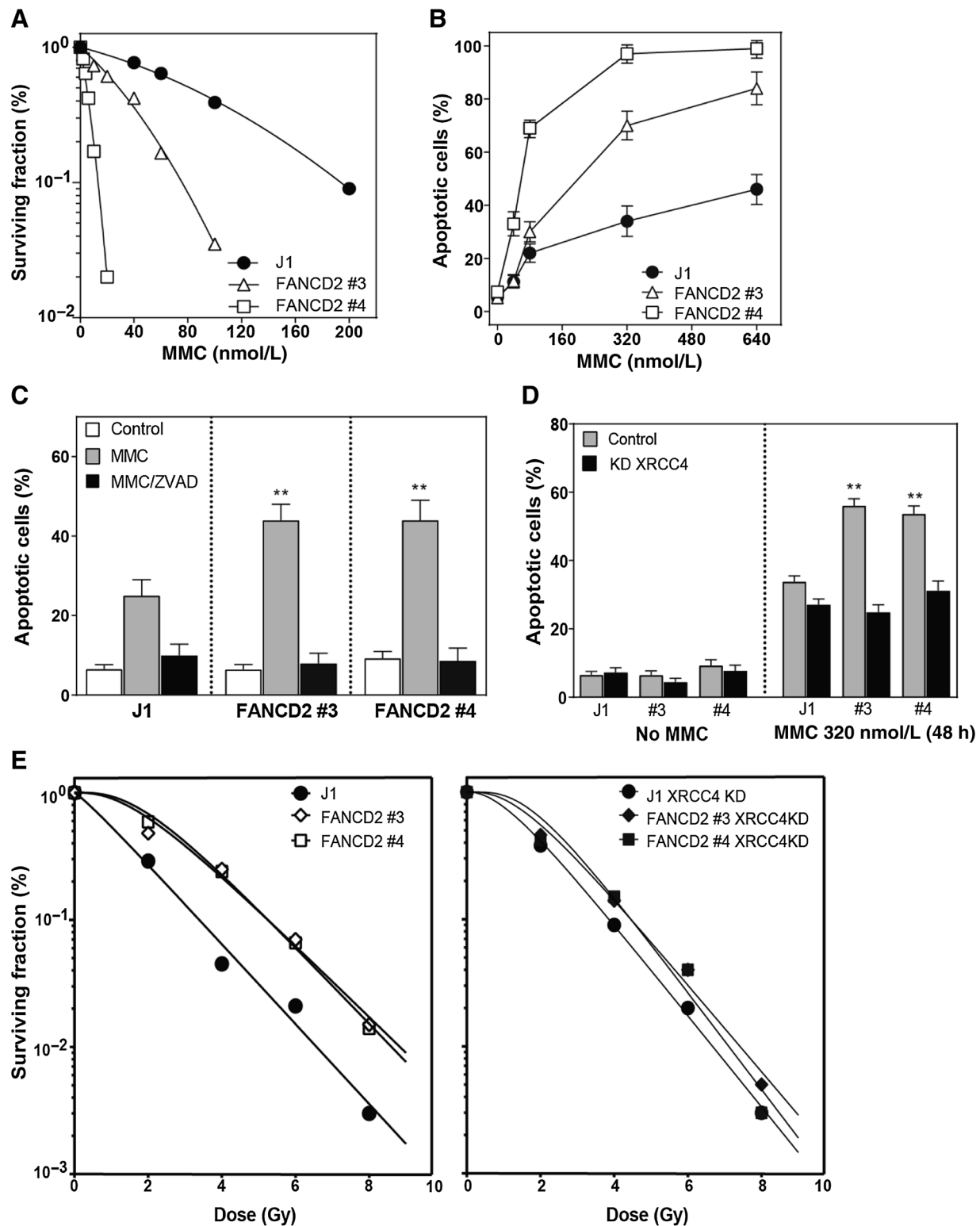
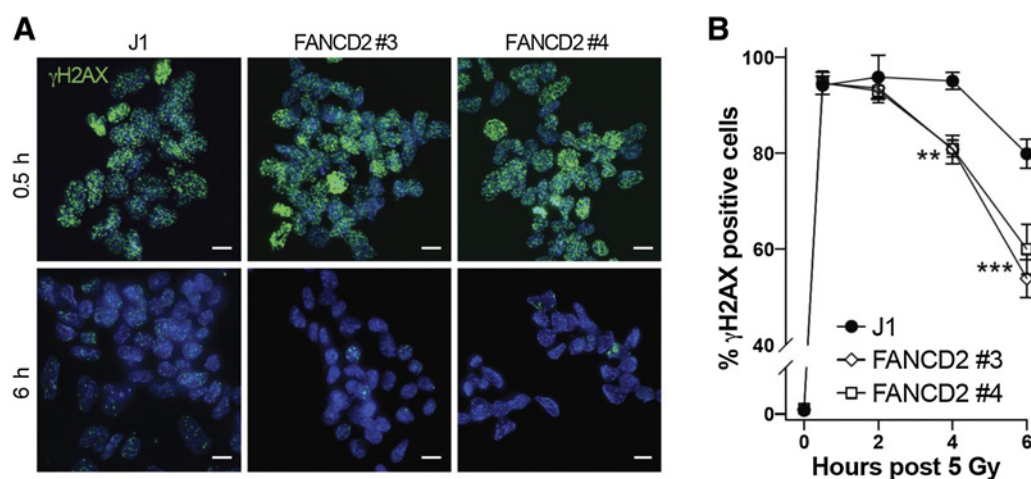


Figure 4.

DNA damage response in FANCD2-deficient mouse ES cells. **A-C**, FANCD2-deficient ES cells were ICL sensitive, measured after MMC by surviving colonies in a clonogenic assay (**A**) or apoptosis by *bis*-benzamide staining (**B**) inhibitable by the caspase-inhibitor ZVAD (100  $\mu$ M/L; **C**). **D**, Knockdown (KD) mouse XRCC4 blocks MMC-induced incremental apoptotic enhancement in FANCD2-deficient ES cells, performed as in **C**. Data are from three triplicate experiments (**A**). Data (mean  $\pm$  SD) are from two (**C**) or three (**D**) triplicate experiments. \*\*,  $P \leq 0.01$ . **E**, Irradiation of FANCD2-deficient ES cells shows relative resistance, which is dependent on XRCC4.

Deng et al.

**Figure 5.**

FANCD2 deficiency facilitates the kinetics of  $\gamma$ H2AX foci resolution. **A**, Representative immunofluorescent images of  $\gamma$ H2AX foci in wild-type and FANCD2-deficient mouse ES cells at 0.5 and 6 hours after 5 Gy irradiation. Cells were counterstained with DAPI. Scale bars, 10  $\mu$ m. **B**, Quantification data of **A** show FANCD2-deficient mouse ES cells resolve irradiation-induced  $\gamma$ H2AX foci much faster than wild-type cells after irradiation. Data presented are (mean  $\pm$  SEM); total  $n = 1,450$  cells (J1), 1,664 cells (FANCD2#3), and 1,263 cells (FANCD2#4). \*\*,  $P < 0.01$ ; \*\*\*,  $P < 0.001$  versus wild-type control,  $t$  test.

nor human fibroblasts with defective Fanconi anemia show significant differences in radiation survival. For example, human FancD2-deficient fibroblast cells, compared with complemented cells show no difference in survival after ionizing radiation (38). Furthermore, Schindler and co-workers compared normal fibroblasts with Fanconi anemia fibroblasts from complementation groups A, C, and G and found no difference in colony formation or cell growth after exposure to ionizing radiation (39). In addition, no difference in radiation survival was found in genetically defined mouse fibroblasts between wild-type and Fanconi anemia null FancA or FancC cells (40). Similarly, we recently published using U2OS human osteosarcoma cells that depletion of FA-D2 or FA-G did not affect the radiation dose survival curve (37). Whether this phenotype is confined to germline/ES cells or may extend to adult stem cell populations is currently unknown.

We recently published a report detailing the reason that NHEJ is not engaged in the wild-type *C. elegans* gonad upon exposure to ionizing radiation (17). Despite preferential enrichment of NHEJ enzymes (cku-80, lig-4, sir-2.1) throughout the *C. elegans* germline compared with somatic cells, the evidence indicates that NHEJ activation upon DNA damage is actively repressed by an unknown mechanism. Here we identify the mechanism of repression as conferred by Fanconi anemia proteins. In replicating cells, a body of evidence suggests that the Fanconi anemia complex “chaperones” ICL intermediates such that Ku cannot bind to the DSB created by ICL processing (10). However, when Fanconi anemia is absent, NHEJ acts on broken replication forks to produce DSBs, which are not joined at the original site, but instead are used to produce the chromosomal aberrations characteristic of Fanconi anemia. As apoptosis is not available in the mitotic compartment of the distal gonad, it appears that cells must enter meiosis to initiate NHEJ-dependent apoptosis. Note that while the mechanism of suppression of apoptosis in the mitotic compartment is currently unknown, our recent manuscript (17) represents perhaps the most detailed analysis of this compartmentalization of apoptotic death in the *C. elegans* gonad. Conversely, in contrast to wild-type DSB repair by homologous recombination after ionizing radiation, in the absence of Fanconi

anemia proteins and with lack of apoptosis availability, NHEJ engagement in the mitotic compartment yields inappropriate DNA repair. Whether incapacity to undergo NHEJ-mediated apoptosis plays any role in conversion to NHEJ-mediated DNA DSB repair is currently unknown, and will require substantial effort to uncover in the future.

The relative contribution of NHEJ to defects in Fanconi anemia cells has been a recent topic of interest. La Volpe and colleagues (9) suggested that NHEJ contributes to *C. elegans* embryonic lethality to crosslinking agents, but did not address differences between cross-links and ionizing radiation (or replication-associated DSBs), nor examine survival in the different cellular compartments of the worm. Patel and co-workers (10) provided evidence that ICL sensitivity and an HR defect of the FANCC knockout of DT40 cells were partially rescued by additional *Ku70* knockout. In this study, Fanconi anemia proteins were found to interfere with the ability of Ku70 to bind DSB ends, thereby limiting NHEJ activity in wild-type cells compared with Fanconi anemia-deficient cells. However, these studies did not find rescue of ICL sensitivity with knockout of DNA-dependent protein kinase (*DNA-PK*) or *Ligase IV*, which differs from the article by La Volpe and colleagues, and from what we found in the current paper together with our earlier work (37). Overall, we favor the view that any component of NHEJ, when inactivated, can rescue the ICL sensitivity of Fanconi anemia cells or animals. Other work in this domain also supports the view that Fanconi anemia proteins are inhibiting end-joining, such that Fanconi anemia cells are associated with interchromosomal junctions that lack homology, as reported by Newell and colleagues (41).

More recent work from Pang and co-workers (42) suggests that Fanconi anemia hematopoietic stem cells (HSC) when treated with ICL-producing agents plus a DNA-PK inhibitor actually have worse survival, findings for this cell lineage that differ from the above reports. The same group (43) showed that DNA-PKc inhibition sensitizes FancA<sup>-/-</sup> HSCs to PARP inhibitor (PARPi)-induced cell death, consistent with our observations that type of DNA damage matters. After PARP inhibition, the predominant life-threatening lesion is the broken

replication fork or daughter strand break, which needs NHEJ for repair and survival. In the same article, when a Fanconi anemia/PARP double knockout line was treated with an ICL agent such as MMC, then the DNA-PK inhibitor produces increased cell killing. In other words, the loss of PARP1 changes the response to ICLs, such that the processing of the ICLs produces repair intermediates that now require NHEJ for survival. Whether these observations are specific to HSCs or whether they are due to the combination of therapies is not fully resolved. We think that the DNA damage, that is modified by the loss of PARP function, is the major driver of these findings, with cell lineage primarily determining the mode of cell death.

The lineage questions are clearly complex: loss of DNA-PK activity by use of a triple-alanine phosphorylation site mutant (43) results in hematopoietic lethality when crossed into a Fanconi anemia mouse, suggesting that NHEJ allows HSCs to survive normal replication cycling, which will produce a small number of DSBs. However, the triple-alanine mutant may also be a block to DSB repair of any type, because it locks DNA-PK at the DSB end (trapping) without the correct processing and hence there are no pathways available to repair intermediates of spontaneous cross-links.

The current study suggests that the nature of the DNA damage is critical to determining outcome. Consistent with this notion, we previously showed using pharmacologic blockade that DNA-PK inhibition after MMC promoted survival of Fanconi anemia-depleted U2OS cells, whereas the same inhibitor after ionizing radiation (plus or minus a PARP-) in the same cell promoted cell death (37). These pharmacologic studies are conceptually similar to the genetic data in the current study that shows in the Fanconi anemia setting NHEJ promotes some types of DNA-damaged mediated lethality, while preventing other types. In summary, the key findings of the current investigation are that after ICL treatment, NHEJ promotes lethality by producing chromosomal aberrations and promoting apoptosis, whereas after ionizing radiation, active NHEJ allows survival, particularly in the stem cell compartment, where apoptotic machinery is inactive. We propose that evaluation of NHEJ-dependent radioresistance in the ES cell-like population that is enriched in Fanconi anemia squamous cell carcinoma of the head and neck (HNSCC) specimens compared with sporadic HNSCC (44) would be an excellent model to test whether our concepts translate into Fanconi anemia cancer models. In this context, Fanconi anemia HNSCC is highly aggressive and radioresistant compared with human papillomavirus-positive

HNSCC (45). Additional detailed investigations are required to further delineate fundamental principles associated with these findings.

### Authors' Disclosures

D.S. Higginson reports grants from NCI, Emerson Collective Cancer Research Fund, AACR, and Clinical Translational Science Center during the conduct of the study; grants from SQZ Biotechnologies and other support from Bio-Rad, Inc. outside the submitted work; in addition, D.S. Higginson has a patent for Compositions & Methods for Monitoring DNA Repair pending. L. Studer reports grants from NCI during the conduct of the study; other support from BlueRock Therapeutics; grants from National Institute of Aging, National Institute of Neurological Disease and Stroke, New York Stem Cell Science (NYSTEM), JPB Foundation, Melanoma Research Foundation, Starr Foundation, and Aligning Research Across Parkinson's disease (ASAP) outside the submitted work. S.N. Powell reports personal fees from Varian, Phillips, Rain Therapeutics, and AstraZeneca outside the submitted work. Z. Fuks reports other support from Ceramedix Holding LLC outside the submitted work. R. Kolesnick reports grants from NIH/NCI during the conduct of the study and other support from Ceramedix Holding LLC outside the submitted work. No disclosures were reported by the other authors.

### Authors' Contributions

**X. Deng:** Data curation, formal analysis, investigation, visualization, methodology, writing—original draft, writing—review and editing. **J. Tchieu:** Data curation, software, formal analysis. **D.S. Higginson:** Formal analysis, validation. **K.-S. Hsu:** Software. **R. Feldman:** Data curation, formal analysis. **L. Studer:** Formal analysis, validation. **S. Shaham:** Formal analysis, validation. **S.N. Powell:** Formal analysis, validation. **Z. Fuks:** Conceptualization, formal analysis, supervision, validation, methodology, writing—review and editing. **R. Kolesnick:** Conceptualization, resources, data curation, software, formal analysis, supervision, funding acquisition, validation, investigation, visualization, methodology, writing—original draft, project administration, writing—review and editing.

### Acknowledgments

We are grateful to Caenorhabditis Genetics Center, Zhirong Bao, Xue Ding, and Iva Greenwald for providing *C. elegans* strains, Markus Grompe for mouse FANCD2 knockout ES cells, and Sang-gyu Lee, John Fuller, David Michaelson and the Molecular Cytology Core Facility of MSKCC for technical support. All data described in this article are available in the main text and Supplementary Materials and Methods.

This work was supported in part through the NIH/NCI Cancer Center Support Core Grant P30 CA008748 to MSKCC.

The costs of publication of this article were defrayed in part by the payment of page charges. This article must therefore be hereby marked *advertisement* in accordance with 18 U.S.C. Section 1734 solely to indicate this fact.

Received October 1, 2020; revised March 15, 2021; accepted April 28, 2021; published first May 3, 2021.

### References

- Fanconi G. Familial constitutional pancytopenia, Fanconi's anemia (F.A.). I. Clinical aspects. *Semin Hematol* 1967;4:233–40.
- Ceccaldi R, Sarangi P, D'Andrea AD. The Fanconi anaemia pathway: new players and new functions. *Nat Rev Mol Cell Biol* 2016;17:337–49.
- Moldovan GL, D'Andrea AD. FANCD2 hurdles the DNA interstrand crosslink. *Cell* 2009;139:1222–4.
- Joenje H, Patel KJ. The emerging genetic and molecular basis of Fanconi anaemia. *Nat Rev Genet* 2001;2:446–57.
- Kottemann MC, Smogorzewska A. Fanconi anaemia and the repair of Watson and Crick DNA crosslinks. *Nature* 2013;493:356–63.
- Kee Y, D'Andrea AD. Molecular pathogenesis and clinical management of Fanconi anemia. *J Clin Invest* 2012;122:3799–806.
- Youds JL, Barber LJ, Boulton SJ. *C. elegans*: a model of Fanconi anemia and ICL repair. *Mutat Res* 2009;668:103–16.
- Collis SJ, Barber LJ, Ward JD, Martin JS, Boulton SJ. *C. elegans* FANCD2 responds to replication stress and functions in interstrand cross-link repair. *DNA Repair* 2006;5:1398–406.
- Adamo A, Collis SJ, Adelman CA, Silva N, Horejsi Z, Ward JD, et al. Preventing nonhomologous end joining suppresses DNA repair defects of Fanconi anemia. *Mol Cell* 2010;39:25–35.
- Pace P, Mosedale G, Hodskinson MR, Rosado IV, Sivasubramanian M, Patel KJ. Ku70 corrupts DNA repair in the absence of the Fanconi anemia pathway. *Science* 2010;329:219–23.
- Brenner S. The genetics of *Caenorhabditis elegans*. *Genetics* 1974;77:71–94.
- Pepper AS, Killian DJ, Hubbard EJ. Genetic analysis of *Caenorhabditis elegans* glp-1 mutants suggests receptor interaction or competition. *Genetics* 2003;163:115–32.
- Park EC, Horvitz HR. Mutations with dominant effects on the behavior and morphology of the nematode *Caenorhabditis elegans*. *Genetics* 1986;113:821–52.
- Mapes J, Chen YZ, Kim A, Mitani S, Kang BH, Xue D. CED-1, CED-7, and TTR-52 regulate surface phosphatidylerine expression on apoptotic and phagocytic cells. *Curr Biol* 2012;22:1267–75.
- Du Z, Santella A, He F, Tiongson M, Bao Z. *De novo* inference of systems-level mechanistic models of development from live-imaging-based phenotype analysis. *Cell* 2014;156:359–72.

Deng et al.

16. Beifuss KK, Gumienny TL. RNAi screening to identify postembryonic phenotypes in *C. elegans*. *J Vis Exp* 2012:e3442. DOI: 10.3791/3442.
17. Deng X, Michaelson D, Tchieu J, Cheng J, Rothenstein D, Feldman R, et al. Targeting homologous recombination in notch-driven *C. elegans* stem cell and human tumors. *PLoS One* 2015;10:e0127862.
18. Harris J, Lowden M, Clejan I, Tzoneva M, Thomas JH, Hodgkin J, et al. Mutator phenotype of *Caenorhabditis elegans* DNA damage checkpoint mutants. *Genetics* 2006;174:601–16.
19. Huumonen K, Immonen HK, Baverstock K, Hiltunen M, Korkalainen M, Lahtinen T, et al. Radiation-induced genomic instability in *Caenorhabditis elegans*. *Mutat Res* 2012;748:36–41.
20. Bocker W, Iliakis G. Computational methods for analysis of foci: validation for radiation-induced gamma-H2AX foci in human cells. *Radiat Res* 2006;165:113–24.
21. Franken NA, Rodermond HM, Stap J, Haveman J, van Bree C. Clonogenic assay of cells *in vitro*. *Nat Protoc* 2006;1:2315–9.
22. Nomiya T. Discussions on target theory: past and present. *J Radiat Res* 2013;54:1161–3.
23. Stancevic B, Varda-Bloom N, Cheng J, Fuller JD, Rotolo JA, Garcia-Barros M, et al. Adenoviral transduction of human acid sphingomyelinase into neo-angiogenic endothelium radiosensitizes tumor cure. *PLoS One* 2013;8:e69025.
24. Altman DG, Bland JM. How to obtain the confidence interval from a P value. *BMJ* 2011;343:d2090.
25. Lee KY, Yang I, Park JE, Baek OR, Chung KY, Koo HS. Developmental stage- and DNA damage-specific functions of *C. elegans* FANCD2. *Biochem Biophys Res Commun* 2007;352:479–85.
26. Youds JL, Barber LJ, Ward JD, Collis SJ, O'Neil NJ, Boulton SJ, et al. DOG-1 is the *Caenorhabditis elegans* BRIP1/FANCD2 homologue and functions in interstrand cross-link repair. *Mol Cell Biol* 2008;28:1470–9.
27. Gartner A, Milstein S, Ahmed S, Hodgkin J, Hengartner MO. A conserved checkpoint pathway mediates DNA damage-induced apoptosis and cell cycle arrest in *C. elegans*. *Mol Cell* 2000;5:435–43.
28. Huang L, Snyder AR, Morgan WF. Radiation-induced genomic instability and its implications for radiation carcinogenesis. *Oncogene* 2003;22:5848–54.
29. Little JB. Radiation carcinogenesis. *Carcinogenesis* 2000;21:397–404.
30. Houghtaling S, Timmers C, Noll M, Finegold MJ, Jones SN, Meyn MS, et al. Epithelial cancer in Fanconi anemia complementation group D2 (Fancd2) knockout mice. *Genes Dev* 2003;17:2021–35.
31. Tichy ED, Pillai R, Deng L, Liang L, Tischfield J, Schwemberger SJ, et al. Mouse embryonic stem cells, but not somatic cells, predominantly use homologous recombination to repair double-strand DNA breaks. *Stem Cells Dev* 2010;19:1699–711.
32. Goodarzi AA, Jeggo PA. Irradiation induced foci (IRIF) as a biomarker for radiosensitivity. *Mutat Res* 2012;736:39–47.
33. Rosenberg PS, Greene MH, Alter BP. Cancer incidence in persons with Fanconi anemia. *Blood* 2003;101:822–6.
34. Nalepa G, Clapp DW. Fanconi anaemia and cancer: an intricate relationship. *Nat Rev Cancer* 2018;18:168–85.
35. Michl J, Zimmer J, Tarsounas M. Interplay between Fanconi anemia and homologous recombination pathways in genome integrity. *EMBO J* 2016;35:909–23.
36. Liu TX, Howlett NG, Deng M, Langenau DM, Hsu K, Rhodes J, et al. Knockdown of zebrafish Fancd2 causes developmental abnormalities via p53-dependent apoptosis. *Dev Cell* 2003;5:903–14.
37. Eccles LJ, Bell AC, Powell SN. Inhibition of non-homologous end joining in Fanconi Anemia cells results in rescue of survival after interstrand crosslinks but sensitization to replication associated double-strand breaks. *DNA Repair* 2018;64:1–9.
38. Kuhnert VM, Kachnic LA, Li L, Purschke M, Gheorghiu L, Lee R, et al. FANCD2-deficient human fibroblasts are hypersensitive to ionising radiation at oxygen concentrations of 0% and 3% but not under normoxic conditions. *Int J Radiat Biol* 2009;85:523–31.
39. Kalb R, Duerr M, Wagner M, Herterich S, Gross M, Digweed M, et al. Lack of sensitivity of primary Fanconi's anemia fibroblasts to UV and ionizing radiation. *Radiat Res* 2004;161:318–25.
40. Noll M, Battaile KP, Bateman R, Lax TP, Rathbun K, Reifsteck C, et al. Fanconi anemia group A and C double-mutant mice: functional evidence for a multi-protein Fanconi anemia complex. *Exp Hematol* 2002;30:679–88.
41. Newell AE, Akkari YM, Torimaru Y, Rosenthal A, Reifsteck CA, Cox B, et al. Interstrand crosslink-induced radials form between non-homologous chromosomes, but are absent in sex chromosomes. *DNA Repair* 2004;3:535–42.
42. Du W, Amarachintha S, Wilson AF, Pang Q. Hyper-active non-homologous end joining selects for synthetic lethality resistant and pathological Fanconi anemia hematopoietic stem and progenitor cells. *Sci Rep* 2016;6:22167.
43. Nie Y, Li Y, Li X, Wilson AF, Pang Q. The non-homologous end-joining activity is required for Fanconi anemia fetal HSC maintenance. *Stem Cell Res Ther* 2019;10:114.
44. Wu J, Mu Q, Thiviyanathan V, Annapragada A, Vigneswaran N. Cancer stem cells are enriched in Fanconi anemia head and neck squamous cell carcinomas. *Int J Oncol* 2014;45:2365–72.
45. Kutler DI, Auerbach AD, Satagopan J, Giampietro PF, Batish SD, Huvos AG, et al. High incidence of head and neck squamous cell carcinoma in patients with Fanconi anemia. *Arch Otolaryngol Head Neck Surg* 2003;129:106–12.

# Cancer Research

The Journal of Cancer Research (1916–1930) | The American Journal of Cancer (1931–1940)

## Disabling the Fanconi Anemia Pathway in Stem Cells Leads to Radioresistance and Genomic Instability

Xinzhu Deng, Jason Tchieu, Daniel S. Higginson, et al.

*Cancer Res* 2021;81:3706-3716. Published OnlineFirst May 3, 2021.

**Updated version** Access the most recent version of this article at:  
doi:[10.1158/0008-5472.CAN-20-3309](https://doi.org/10.1158/0008-5472.CAN-20-3309)

**Supplementary Material** Access the most recent supplemental material at:  
<http://cancerres.aacrjournals.org/content/suppl/2021/04/30/0008-5472.CAN-20-3309.DC1>

**Cited articles** This article cites 44 articles, 10 of which you can access for free at:  
<http://cancerres.aacrjournals.org/content/81/13/3706.full#ref-list-1>

**E-mail alerts** [Sign up to receive free email-alerts](#) related to this article or journal.

**Reprints and Subscriptions** To order reprints of this article or to subscribe to the journal, contact the AACR Publications Department at [pubs@aacr.org](mailto:pubs@aacr.org).

**Permissions** To request permission to re-use all or part of this article, use this link  
<http://cancerres.aacrjournals.org/content/81/13/3706>.  
Click on "Request Permissions" which will take you to the Copyright Clearance Center's (CCC) Rightslink site.